Turbulent Rayleigh-Taylor instability experiments with variable acceleration

Guy Dimonte and Marilyn Schneider
Lawrence Livermore National Laboratory, Livermore, California 94551

(Received 24 January 1996; revised manuscript received 26 April 1996)

Turbulent mixing due to the Rayleigh-Taylor instability is experimentally found to vary strongly with the temporal acceleration profile $g(t)$. For constant g, the bubble amplitude h_b increases as gt^2 consistent with previous results. For sustained acceleration profiles with $dg/dt \neq 0$, h_b increases, not with the displacement $Z = \iint g\ dt'dt$, but with the length $S = 0.5\ [\int \sqrt{g}\ \ dt]^2$. For an impulsive acceleration, mixing is minimized with $h_b \sim Z^{0.4}$. These results are used to test mix models. [S1063-651X(96)12410-7]

PACS number(s): 47.20.Bp, 47.27.Jv

When a fluid of density ρ_1 accelerates another fluid of density ρ_2, hydrodynamic instabilities at the interface enhance the interfluid mixing. Two such instabilities are the Rayleigh-Taylor [1] (RT) instability for a sustained acceleration and the Richtmyer-Meshkov [2] (RM) instability for an impulsive acceleration $g = U\delta(t)$ from a shock. Both instabilities are important in inertial confinement fusion (ICF) because they can produce enough mixing [3,4] to contaminate, cool, and degrade the yield of the thermonuclear fuel. They also affect the evolution of supernova explosions [5].

Both instabilities evolve through three stages, each with characteristic scales and growth rates. First, small amplitude modes grow independently with growth rates and wavelengths determined by the respective linear theory [1,2,6–10]. Second, when the amplitude of a mode becomes comparable to its wavelength, weak nonlinearities reduce the penetration rates [6,7,9–15]. In the third stage, the perturbations have large amplitudes with a broad range of scales. Here, the nonlinearities are strong and the mixing is turbulent [13–18].

Turbulent mixing rates [17–20] have been measured for a constant acceleration and an Atwood ratio $A = (\rho_2 - \rho_1)/(\rho_2 + \rho_1) > 0$. The light fluid is found to penetrate the heavy fluid as bubbles with an amplitude $h_b = \alpha_b Agt^2$ with an empirical constant $\alpha_b \sim 0.06$. Similarly, the heavy fluid penetrates the light fluid as spikes with a parameter $\alpha_s \sim 1 - 3\alpha_b$ that depends on A. Direct numerical simulations (DNS) [18,20–22] reproduce this scaling for h_b, but with a range of values $\alpha_b \sim 0.035–0.07$ depending on the initial amplitudes and the use of interface tracking. Since DNS cannot resolve the full range of turbulent scales, reduced mix models [3,4,13–16,18,21–27] are also used for subgrid modeling and ICF design, but they are empirical and need verification.

It is important to investigate different acceleration profiles because diverse calculations can all reproduce the constant g result, yet the acceleration is variable in most applications [3,5]. Additional applications are discussed in Ref. [28]. As an example, with a varying but sustained acceleration $g \neq 0$, h_b is thought [14,17–19] to increase with the length $S = 0.5$ $[\int \sqrt{g}\ dt]^2$ rather than the displacement $Z = \iint g\ dt'\ dt$. This hypothesis cannot be tested with a constant g since $S = Z = 0.5gt^2$. An impulsive g is particularly useful because S is constant during the coast phase while Z increases as Ut. In this case, turbulence models [24,25] predict that $h_b \sim Z^{\theta_b}$ with $\theta_b \sim \frac{1}{3}$ for bubbles. A large structure model [14,15] predicts $\theta_b \sim 0.4$ for bubbles and, for spikes, an exponent $0.4 < \theta_s < 1$ that depends on A. The transition to the power law [14] occurs when g decays faster than $1/t^2$. Laser RM experiments [29] at $A = -0.87$ obtain an exponent ~ 0.6, but for the combined bubble and spike amplitude because of diagnostic limitations. Shock tubes [30,31] obtain exponents ~ 1.0, but they suffer from membrane and edge effects. Experiments [32] with liquids investigated impulsive g profiles, but with imposed sinusoidal perturbations in two dimensions. Laser Rayleigh-Taylor (RT) experiments [28] use shaped accelerations, but they reach only the weakly nonlinear regime.

We describe turbulent mix experiments with four qualitatively different acceleration profiles using a linear electric motor (LEM) that produce different mixing rates. These extend previous experiments [17–19] with constant g that have been used to test reduced mix models, such as in ICF [23]. Our experiments show that the mixing rate depends strongly on the acceleration profile. Moreover, it is important to vary $g(t)$ to not only calibrate the strength of particular terms in the reduced mixing models, but to test their validity and form.

The LEM [33] is depicted in Fig. 1. A force $F \sim 2I_rDB$ is applied by two armatures of length $D = 10$ cm that slide along four linear electrodes (rails). The magnetic field B is produced by the rail/armature current $I_r < 30$ kA ($\sim 25\%$) and a pair of elongated coils with current $I_c < 60$ kA (75%). A

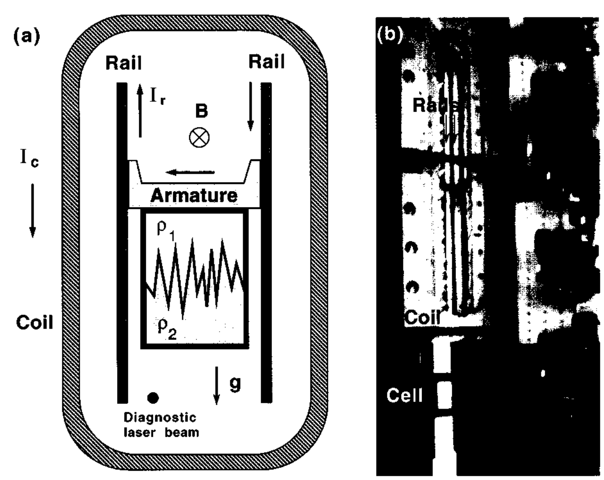

FIG. 1. Schematic (a) and photograph (b) of LEM.

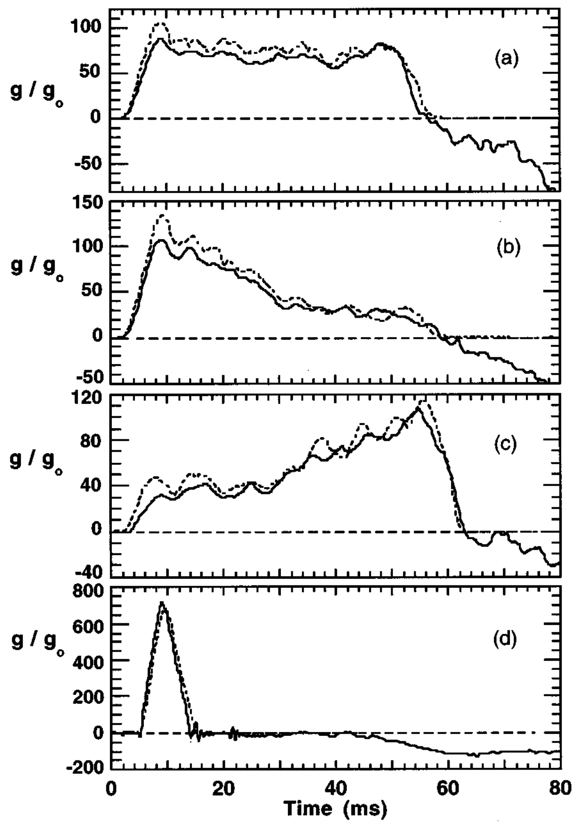

FIG. 2. Acceleration for (a) constant, (b) decreasing, (c) increasing, and (d) impulsive profiles. Solid lines are measured and dashed lines are calculated. The final velocities are $U \sim 33$, 27, 31, and 34 m/s for (a)–(d), respectively.

total energy of 0.6 MJ is available in 16 independent capacitor banks ($450 v$, $0.36 f$ each) with different charge voltages and discharge times for pulse shaping. The projectile has a fluid cavity (7.3 cm wide, 7.3 cm deep, 8.8 cm long) and a mass of $\sim$1.8 kg. Transverse laser beams are used to measure the cell trajectory $Z(t)$ and to trigger optical backlighters (5 μs).

The acceleration profiles in Fig. 2 are studied because they have different values of S/Z, yet they produce the same final velocity $U \sim 31$ m/s. The acceleration measured with a piezoresistive accelerometer (solid) is typically smaller than that calculated using I_r and I_c (dashed) because of friction. For Fig. 2(a), the average values are $g \sim 70 g_0$ (g_0=earth's gravity), $I_r \sim 11$ kA, $I_c \sim 20$ kA, and $B \sim 0.8$ T. The variations $\delta g/g < \pm 15\%$ are not important and $S \sim Z \pm 3\%$. For the decreasing accelerating profile [Fig. 2(b)], $S/Z \sim 1$ for $Z < 25$ cm and then decreases to $S/Z \sim 0.74$ by $Z = 95$ cm. The increasing profile (Fig. 2c) has $S/Z \sim 1.27$ throughout. For the impulsive profile [Fig. 2(d)], $S \sim Z$ during the acceleration, but S remains constant $\sim$15 cm during the coast phase whereas Z increases to 130 cm. For technical reasons, the acceleration begins at 2 ms for the sustained profiles and 5 ms for the impulsive profile.

The evolution of the mixing zone for the constant acceleration case is shown in Fig. 3. The fluids are immiscible: Freon ($\rho_2 = 1.57$ g/cm^3) on the bottom and water ($\rho_1 = 1$ g/cm^3) on top. A surfactant is added to reduce the surface tension ($T \sim 1.4$ dynes/cm) and the meniscus at the walls (<1 mm in amplitude and extent). The mix region is dark because the fluids have different indices of refraction and scatter the light in the turbulent region. The data in Fig. 3(a)–3(e) is characterized in the same way as in the original experiments [17–20]; namely, h_b is defined by the fastest growing bubbles as indicated by the dotted line in Fig. 3(d). Other characterizations such as using the average location of the envelope of the interface for h_b may be preferable, but its meaning would differ from that in the original papers and comparisons would be compromised.

The interface is initially flat and glassy as indicated by perspective views. In Fig. 3(b)–3(e), h_b increases $\sim$0.21, 1, 1.85, and 2.2 cm linearly with the displacement as expected from turbulence scaling since the Reynolds number exceeds 10^6. At the same time, the bubbles also increase their average diameter $D_b \sim 0.11$, 0.37, 0.72, and 0.83 cm, suggesting a self-similar evolution with $h_b \sim 3\ D_b$. Even by 12 ms, the instability has evolved well beyond the linear regime [8]. With surface tension, the fastest growing wavelength is $\lambda_m \sim 2\pi[3T/g(\rho_1 - \rho_2)]^{1/2} \sim 0.06$ cm with an e-fold time $\tau_e \sim (3\lambda_m/4\pi A g)^{1/2} \sim 1$ ms. This mode would have exponentiated to $h_b \sim 2$ cm$\sim 30\ \lambda_m$ (with $h_b \sim 1$ μm initially) which is 10$\times$ larger than observed. Figure 3(f) is a perspec-

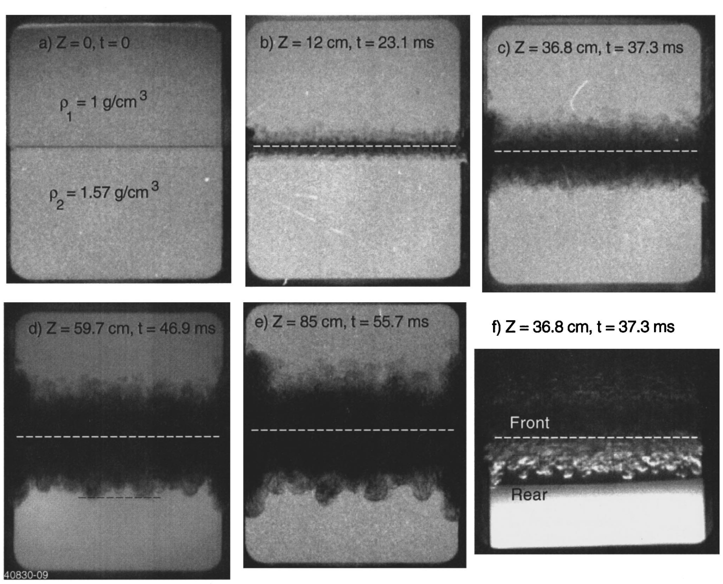

FIG. 3. (a)–(e) Shadowgraphs for constant acceleration profile at different times and locations for Freon and water (A=0.22). The white dashed lines indicate the initial interface and the black dashed line exemplifies a bubble amplitude h_b. (f) Perspective image from 12° below the interface at Z=36.8 cm. To indicate the scale, the fluid cavity is 7.3 cm wide and 8.8 cm tall.

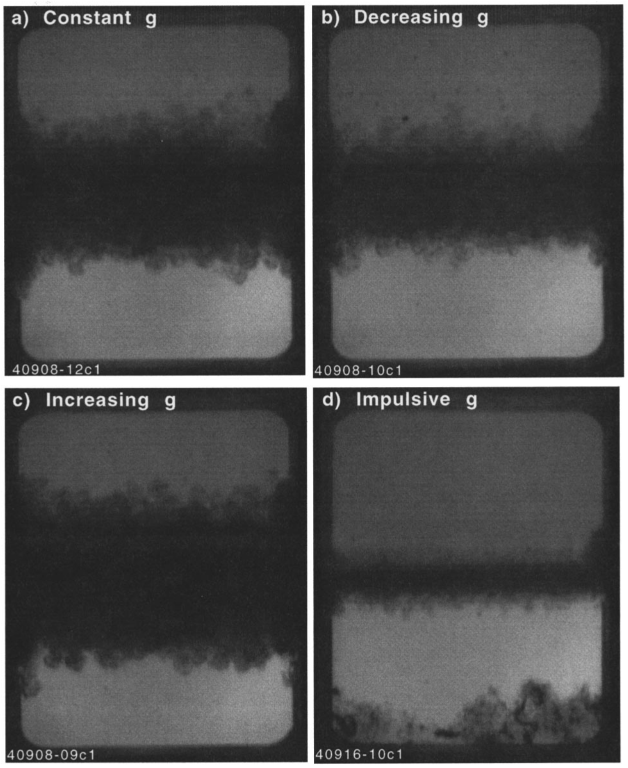

FIG. 4. Shadowgraphs for the acceleration profiles in Fig. 2 at similar locations for $A=0.22$. (a) $Z=68.3$ cm; $t=48.3$ ms, (b) $Z=68.3$ cm, $t=48.7$ ms, (c) $Z=68.3$ cm, $t=59.2$ ms, and (d) $Z=69.6$ cm, $t=30.3$ ms. To indicate the scale, the fluid cavity is 7.3 cm wide and 8.8 cm tall.

tive image at $Z=36.8$ cm from 12° below the interface and it indicates that the bubbles are three dimensional; namely, they are round and randomly distributed in the transverse dimensions and elongated in the acceleration direction. The spike penetrations are 10–20 % larger than for the bubbles as seen previously [17–20] for low A.

Tests were conducted to check the experimental integrity. We varied the size of the meniscus and found very little difference in the instability amplitude in the center. The meniscus is more important for $A\sim1$, particularly in the corners. The effect of vibration was evaluated by accelerating the cell upwards in the stable direction ($gA<0$). No perturbations were observed until the fluids entered the brake region and became RT unstable ($gA>0$).

The mixing produced by our four acceleration profiles is shown in Fig. 4 with $A=0.22$. The displacements are similar $Z=68.3$ and 69.6 cm, but $h_b\sim1.82$, 1.67, 2.3, and 1 cm, and $S\sim69.9$, 54.3, 84.6, and 15 cm are different in Figs. 4(a)–4(b), respectively. The mixing zone is largest for the increasing acceleration profile ($dg/dt>0$) and smallest for the impulsive profile. The dark region at the bottom of Fig. 4(d) is due to cavitation which occurs for $g>150g_0$ when the minimum pressure falls below the Freon vapor pressure [34]. The cavitation does not seem to affect the mixing at the interface.

Figure 5 shows the bubble penetration depth h_b vs the displacement Z for the four acceleration profiles. For constant g, we find $h_b=\alpha_b Agt^2$ ($Z=0.5gt^2$) with $\alpha_b\sim0.061$, consistent with previous experiments [17–20]. The ratio $h_b/2AZ$ becomes ~0.074 for the increasing profile and ~0.049 for the decreasing profile. For the impulsive case, h_b is not linear with Z and there are two phases. During the 9-ms acceleration phase, the cell is displaced $Z_0\sim15$ cm and $h_{b0}\sim0.4$ cm. During the coast phase $Z>Z_0$, the penetration increases slowly with displacement according to a power law $h_b/h_{b0}\sim(Z/Z_0)^{\theta_b}$ with $\theta_b\sim0.37$. We estimate the error in the data (<10%) from the shot-to-shot variation in Fig. 5.

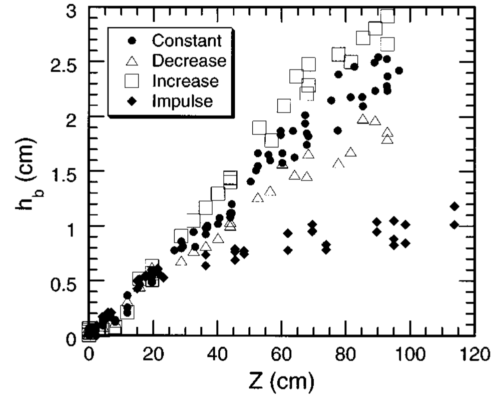

FIG. 5. The bubble penetration distance h_b vs Z for the acceleration profiles in Fig. 2. $A=0.22$.

We evaluate two models with this data. Figure 6(a), shows h_b vs S where S is calculated from the measured acceleration profiles. Most of the data is unified along a single line $h_b=2\alpha_b AS$ with $\alpha_b\sim0.061$. The impulsive case violates this hypothesis during the coast phase, as indicated by the vertical column of data at $S\sim15$ cm, because h_b increases while S is constant. A better description is obtained with a simplified two-phase flow model

$$dV_b/dt=\beta Ag-C_d V_b^2/h_b, \tag{1}$$

where the bubble penetration velocity is $dh_b/dt=V_b$. The form of Eq. (1) is taken from the potential flow model [12] and resembles the equation of motion for a bubble rising through a fluid that exerts a Newtonian drag [11]. It has also been obtained form a large structure model of mixing [14,15]. Youngs [34] postulates that the buoyancy term Ag may be reduced by some factor $\beta<1$ because fluid entrainment in the turbulent region reduces the density contrast. The drag coefficient C_d has been evaluated for isolated bubbles [11] but not for interpenetrating fluids. The denominator in

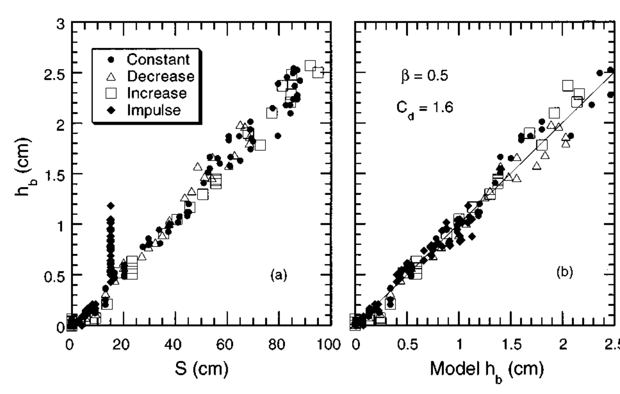

FIG. 6. The measured h_b vs (a) the parameter S and (b) the solution to Eq. (1) for $\beta=0.5$ and $C_d=1.6$. The line is a regression fit.

the drag term represents the ratio of volume to cross-sectional area of a bubble which Layzer took to be its radius $D_b/2$. We use h_b for simplicity based on the observed self-similarity $h_b \sim 3D_b$, but this term is still undetermined and will require further experiments to resolve. For constant g, the solution to Eq. (1) is $h_b = \alpha_b A g t^2$ if $\beta = 2\alpha_b(1+2C_d)$, but the values of β and C_d are not unique. C_d is best determined with an impulsive drive because the solution is $h_b \sim t^{\theta_b}$ with $\theta_b = (1+C_d)^{-1}$.

Numerical solutions to Eq. (1) for our acceleration profiles are compared with measured results in Fig. 6(b) using $\beta = 0.5$ and $C_d = 1.6$. The solutions are not sensitive to the initial conditions $V_b = 0$ and $h_b = 1$ μm [26] (h_b increases by $<10\%$ with 100 μm initial amplitude). Solutions [26] with $\beta = 1$ and $C_d = 3.7$ are inadequate because the exponent is too low $\theta_b = (1+C_d)^{-1} \sim 0.2$, and they would yield $h_b \sim 0.6$ cm at $Z = 100$ cm, which is well below that measured $h_b \sim 1$ cm. With $C_d = 1.6$, the exponent is $\theta_b \sim 0.38$ in accordance with Ref. [15]. The bubble competition model is also consistent with our high laser experiments [29] at $A = -0.87$, which obtained an exponent ~ 0.6 for the combined bubbles and spikes. Different $g(t)$ profiles and Atwood ratios need to be investigated to fully evaluate the mix models [13–27].

In conclusion, turbulent mixing is found to depend strongly on the temporal acceleration profile $g(t)$. For arbitrary but sustained $g(t) \neq 0$, we find that $h_b = 2\alpha_b A S$ with $\alpha_b \sim 0.061$, which reduces to $h_b = \alpha_b A g t^2$ for constant g. This confirms the previous hypothesis [17–19] that S (rather than Z) determines the mixing rate when $g \neq 0$, and it implies that at the same displacement h_b is larger for $dg/dt > 0$ and smaller for $dg/dt < 0$. As an example, the increasing $g(t)$ is shown to be the most hydrodynamically unstable acceleration profile, and this may be important to ICF. Mixing is minimized with an impulsive profile for which h_b obeys the power law $h_b \sim Z^{\theta_b}$ with $\theta_b \sim 0.4$ in accordance with the large structure mix model [14,15]. A mix model exemplified by Eq. (1) can describe the mixing from all the $g(t)$ profiles, but further experiments with more complex $g(t)$ profiles, including some deceleration [34], may be required to develop a more complete description of turbulent mix. These are currently underway.

We thank J. Morrison, S. Hulsey, D. Nelson, and S. Weaver for their excellent technical contributions and V. Smeeton, Yu. Kucherenko, D. Shvarts, D. Sharp, G. Burke, B. Remington, and R. Hawke for useful discussions. We also thank D. L. Youngs for encouragement and insightful suggestions. This work was performed under the auspices of the U.S. Department of Energy by the Lawrence Livermore National Laboratory under Contract No. W-7405-ENG-48.

[1] Lord Rayleigh, Scientific Papers II, (Cambridge, England, 1900), p. 200; G. I. Taylor, Proc. R. Soc. London Ser. A **201**, 192 (1950).

[2] R. D. Richtmyer, Commun. Pure Appl. Math. **13**, 297 (1960); E. E. Meshkov, Izv. Acad. Sci. USSR Fluid Dynamics **4**, 101 (1969).

[3] Steven W. Haan *et al.*, Phys. Plasmas **2**, 2480 (1995).

[4] V. A. Andronov *et al.*, JETP Lett. **29**, 56 (1979).

[5] T. Ebisuzki, T. Shigeyama, and K. Nomoto, Astrophys. J. **344**, L65 (1989).

[6] D. J. Lewis, Proc. R. Soc. London Ser. A **202**, 81 (1950).

[7] H. W. Emmons, C. T. Chang, and B. C. Watson, J. Fluid Mech. **7**, 177 (1960).

[8] R. Bellman and R. H. Pennington, Quart. J. Appl. Math **12**, 151 (1954).

[9] A. N. Aleshin *et al.*, Dokl. Akad. Nauk SSSR **310**, 1105 (1990) [Sov. Phys. Dokl. **35**, 159 (1990)].

[10] Guy Dimonte and Bruce Remington, Phys. Rev. Lett. **70**, 1806 (1993); Guy Dimonte *et al.*, Phys. Plasmas **3**, 614 (1996).

[11] R. M. Davies and G. I. Taylor, Proc. R. Soc. London Ser. A **200**, 375 (1950).

[12] D. Layzer, Astrophys. J. **122**, 1 (1955).

[13] J. A. Zufiria, Phys. Fluids **31**, 440 (1988).

[14] D. Shvarts *et al.*, Phys. Plasmas **2**, 2465 (1995).

[15] U. Alon *et al.*, Phys. Rev. Lett. **74**, 534 (1995).

[16] J. Glimm and D. H. Sharp, Phys. Rev. Lett. **64**, 2137 (1990).

[17] K. I. Read, Physica **12D**, 45 (1984).

[18] D. L. Youngs, Physica **12D**, 32 (1984); Physica D **37**, 270 (1989); Phys. Fluids A **3**, 1312 (1991).

[19] Yu. A Kucherenko *et al.*, in *title*, edited by editor(s), Proceedings of the 3rd International Workshop on Physics Compressible Turbulent Mixing (Abbey of Royaumont, France, 1991), p. 427.

[20] P. F. Linden, J. M. Redondo, and D. L. Youngs, J. Fluid Mech. **265**, 97 (1994).

[21] J. Glimm *et al.*, Phys. Fluids A **2**, 2046 (1990).

[22] N. Freed *et al.*, Phys. Fluids A **3**, 912 (1991).

[23] S. W. Haan, Phys. Rev. A **39**, 5812 (1989).

[24] V. A. Andronov *et al.*, Dokl. Akad. Nauk SSSR **264**, 76 (1982) [Sov. Phys. Dokl. **27**, 393 (1982)].

[25] S. Gauthier and M. Bonnet, Phys. Fluids A **2**, 1685 (1990).

[26] J. C. Hanson *et al.*, Laser and Particle Beams **8**, 51 (1990).

[27] D. C. Besnard *et al.*, Los Alamos National Laboratory Report No. LA-11821-MS, 1990 (unpublished).

[28] B. Remington *et al.*, Phys. Plasmas **2**, 241 (1995).

[29] Guy Dimonte, C. Eric Frerking, and Marilyn Schneider, Phys. Rev. Lett. **74**, 4855 (1995).

[30] M. Brouillette and B. Sturtevant, Physica D **37**, 248 (1989).

[31] B. Sturtevant, in *Shock Tubes and Waves*, edited by H. Gronig (VCH Verlag, Berlin, 1987), p. 89.

[32] J. W. Jacobs and J. M. Sheeley, Phys. Fluids **8**, 405 (1996).

[33] Guy Dimonte *et al.*, Rev. Sci. Instrum. **67**, 302 (1996).

[34] D. L. Youngs (private communication).